Supporting Information for "Unified spectrum of tropical rainfall and waves in a simple stochastic model"

Samuel N. Stechmann[1,2] and Scott Hottovy[3]

Submitted on April 21, 2017
Revised on August 17, 2017
Revised on September 19, 2017

[1]Department of Mathematics, University of Wisconsin–Madison, Madison, Wisconsin, USA.
[2]Department of Atmospheric and Oceanic Sciences, University of Wisconsin–Madison, Madison, Wisconsin, USA.
[3]Department of Mathematics, United States Naval Academy, Annapolis, Maryland, USA

Contents

Introduction

This Supporting Information describes details of the methods for deriving the model equations and determining solutions. The text sections are organized as follows:

Text S1. Derivation of model dynamical core
Text S2. Moisture background profile
Text S3. Comparison with other models
Text S4. Methods for determining model solutions

Text S1. Derivation of model dynamical core

The dynamical core of (1)–(4) of the main text can be derived from the three-dimensional primitive equations, using a modification of the methods of *Stechmann et al.* [2008], with the addition that water vapor $Q(x, y, z, t)$ is also included and expanded in vertical baroclinic modes.

The starting point for the derivation is the three-dimensional primitive equations, in nondimensional units:

$$\begin{aligned} \frac{D\mathbf{U}}{Dt} + y\mathbf{U}^\perp &= -\nabla P \\ \nabla \cdot \mathbf{U} + \frac{\partial W}{\partial z} &= 0 \\ \frac{\partial P}{\partial z} &= \Theta \\ \frac{D\Theta}{Dt} + W &= 0 \\ \frac{DQ}{Dt} - \tilde{Q}W &= 0, \end{aligned} \tag{S1}$$

The nondimensional units are the same as in *Stechmann and Majda* [2015]. The material derivative is

$$\frac{D}{Dt} = \frac{\partial}{\partial t} + \mathbf{U} \cdot \nabla + W\frac{\partial}{\partial z}.$$

Here the horizonal velocity is $\mathbf{U} = (U(x, y, z, t), V(x, y, z, t))$, and ∇ is the horizonal gradient operator: $\mathbf{U}\cdot\nabla = U\partial_x + V\partial_y$. The vertical velocity is W, and the pressure is P. The

Corresponding author: Samuel N. Stechmann, stechmann@wisc.edu

term $y\mathbf{U}^\perp$ represents the Coriolis force, under the equatorial beta-plane approximation, and where $\mathbf{U}^\perp = (-V, U)$. The potential temperature Θ and water vapor mixing ratio Q are anomalies from background states that are linear with respect to height z:

$$\begin{aligned} \theta^{tot} &= \theta_{00} + z + \Theta(x, y, z, t), \\ q^{tot} &= q_{00} - \tilde{Q}z + Q(x, y, z, t), \end{aligned} \tag{S2}$$

where θ_{00} and q_{00} are constants and represent values at the top of the boundary layer at $z = 0$. For a model of this complexity, it is common to consider the fluid as bounded above and below by rigid lids at the bottom of the troposphere ($z = 0$) and the top of the troposphere ($z = \pi$ in nondimensional units). The boundary condition at $z = 0$ and $z = \pi$ is $W = 0$.

As a spectral representation of vertical variations, we use basis functions that take the form of sinusoids:

$$\begin{aligned} &C_0(z) = 1 \\ &C_j(z) = \sqrt{2}\cos(jz), \qquad\qquad S_j(z) = \sqrt{2}\sin(jz), \qquad j = 1, 2, 3, \cdots \end{aligned} \tag{S3}$$

where the upper lid is located at $z = \pi$ in nondimensional units. The inner product is then defined as

$$\langle F(z), G(z)\rangle = \frac{1}{\pi}\int_0^\pi F(z)G(z)\,dz \tag{S4}$$

so that the S's and the C's are orthonormal bases: $\langle S_i, S_j\rangle = \delta_{ij}$ and $\langle C_i, C_j\rangle = \delta_{ij}$. The model variables are expanded as

$$\begin{aligned} \mathbf{U}(x, y, z, t) &= \sum_{j=0}^{\infty} \mathbf{u}_j(x, y, t)C_j(z), & W(x, y, z, t) &= \sum_{j=1}^{\infty} w_j(x, y, t)S_j(z), \\ P(x, y, z, t) &= \sum_{j=0}^{\infty} p_j(x, y, t)C_j(z), & \Theta(x, y, z, t) &= \sum_{j=1}^{\infty} \theta_j(x, y, t)jS_j(z), \\ & & Q(x, y, z, t) &= \sum_{j=1}^{\infty} q_j(x, y, t)jS_j(z). \end{aligned} \tag{S5}$$

Note that the convention here is to expand Θ and Q in the basis $jS_j(z)$, not $S_j(z)$. See Fig. S3 for illustrations of the basis functions.

To derive a simplified model, all variables are assumed to have a truncated form including only the 1st and 2nd baroclinic modes:

$$\begin{aligned} \mathbf{U} &= \mathbf{u}_1C_1 + \mathbf{u}_2C_2, & P &= -\theta_1C_1 - \theta_2C_2, \\ W &= -\nabla\cdot\mathbf{u}_1S_1 - \frac{1}{2}\nabla\cdot\mathbf{u}_2S_2, & \Theta &= \theta_1S_1 + \theta_2 2S_2, \\ & & Q &= q_1S_1 + q_2 2S_2. \end{aligned} \tag{S6}$$

When (S1) are projected onto the 1st and 2nd baroclinic modes, the result is a coupled system of rotating shallow water equations, including moisture:

$$\begin{cases} \dfrac{\partial \mathbf{u}_1}{\partial t} + y\mathbf{u}_1^{\perp} - \nabla\theta_1 &= -\dfrac{1}{\sqrt{2}}\left[\mathbf{u}_1\cdot\nabla\mathbf{u}_2 + \mathbf{u}_2\cdot\nabla\mathbf{u}_1 + 2\mathbf{u}_2\nabla\cdot\mathbf{u}_1 + \dfrac{1}{2}\mathbf{u}_1\nabla\cdot\mathbf{u}_2\right], \\ \dfrac{\partial \theta_1}{\partial t} - \nabla\cdot\mathbf{u}_1 &= -\dfrac{1}{\sqrt{2}}\left[2\mathbf{u}_1\cdot\nabla\theta_2 - \mathbf{u}_2\cdot\nabla\theta_1 + 4\theta_2\nabla\cdot\mathbf{u}_1 - \dfrac{1}{2}\theta_1\nabla\cdot\mathbf{u}_2\right], \\ \dfrac{\partial q_1}{\partial t} + \tilde{Q}\nabla\cdot\mathbf{u}_1 &= -\dfrac{1}{\sqrt{2}}\left[2\mathbf{u}_1\cdot\nabla q_2 - \mathbf{u}_2\cdot\nabla q_1 + 4q_2\nabla\cdot\mathbf{u}_1 - \dfrac{1}{2}q_1\nabla\cdot\mathbf{u}_2\right], \end{cases}$$

$$\begin{cases} \dfrac{\partial \mathbf{u}_2}{\partial t} + y\mathbf{u}_2^{\perp} - \nabla\theta_2 &= -\dfrac{1}{\sqrt{2}}\left[\mathbf{u}_1\cdot\nabla\mathbf{u}_1 - \mathbf{u}_1\nabla\cdot\mathbf{u}_1\right], \\ \dfrac{\partial \theta_2}{\partial t} - \dfrac{1}{4}\nabla\cdot\mathbf{u}_2 &= -\dfrac{1}{2\sqrt{2}}\left[\mathbf{u}_1\cdot\nabla\theta_1 - \theta_1\nabla\cdot\mathbf{u}_1\right], \\ \dfrac{\partial q_2}{\partial t} + \dfrac{\tilde{Q}}{4}\nabla\cdot\mathbf{u}_2 &= -\dfrac{1}{2\sqrt{2}}\left[\mathbf{u}_1\cdot\nabla q_1 - q_1\nabla\cdot\mathbf{u}_1\right]. \end{cases} \tag{S7}$$

In the present paper, this sytem is further simplified by neglecting the 2nd baroclinic mode wind and potential temperature, but retaining both baroclinic modes of water vapor, in recognition of the importance of representing finer details of the vertical structure of water vapor. Neglecting $\mathbf{u}_2$ and θ_2 and their dynamical equations then leads to

$$\begin{aligned} \frac{\partial \mathbf{u}_1}{\partial t} + y\mathbf{u}_1^{\perp} - \nabla\theta_1 &= 0, \\ \frac{\partial \theta_1}{\partial t} - \nabla\cdot\mathbf{u}_1 &= 0, \\ \frac{\partial q_1}{\partial t} + \tilde{Q}\nabla\cdot\mathbf{u}_1 &= -\frac{1}{\sqrt{2}}\left[2\mathbf{u}_1\cdot\nabla q_2 + 4q_2\nabla\cdot\mathbf{u}_1\right], \\ \frac{\partial q_2}{\partial t} &= -\frac{1}{2\sqrt{2}}\left[\mathbf{u}_1\cdot\nabla q_1 - q_1\nabla\cdot\mathbf{u}_1\right]. \end{aligned} \tag{S8}$$

Furthermore, these dynamics are linearized about a resting state ($\mathbf{u}_1 = 0$) with background water vapor state of $q_1 = \bar{q}_1 =$ constant and $q_2 = \bar{q}_2 =$ constant, which leads to

$$\begin{aligned} \frac{\partial \mathbf{u}_1}{\partial t} + y\mathbf{u}_1^{\perp} - \nabla\theta_1 &= 0, \\ \frac{\partial \theta_1}{\partial t} - \nabla\cdot\mathbf{u}_1 &= 0, \\ \frac{\partial q_1}{\partial t} + (\tilde{Q} + 2\sqrt{2}\bar{q}_2)\nabla\cdot\mathbf{u}_1 &= 0, \\ \frac{\partial q_2}{\partial t} - \frac{\bar{q}_1}{2\sqrt{2}}\nabla\cdot\mathbf{u}_1 &= 0. \end{aligned} \tag{S9}$$

Finally, an inverse discrete Fourier transform is used to transform the water vapor equations from vertical mode variables to vertical level variables. The inverse discrete Fourier transform relations can be seen from (S6) and are

$$\begin{aligned} q_{low} &= Q|_{z=\pi/3} = q_1\sqrt{2}\sin\frac{\pi}{3} + q_2 2\sqrt{2}\sin\frac{2\pi}{3}, \\ q_{mid} &= Q|_{z=2\pi/3} = q_1\sqrt{2}\sin\frac{2\pi}{3} + q_2 2\sqrt{2}\sin\frac{4\pi}{3}, \end{aligned} \tag{S10}$$

or

$$q_{low} = \sqrt{\frac{3}{2}}(q_1 + 2q_2),$$
$$q_{mid} = \sqrt{\frac{3}{2}}(q_1 - 2q_2). \tag{S11}$$

Using these linear combinations of q_1 and q_2, the dynamics from (S9) can be written in terms of q_{low} and q_{mid} as

$$\begin{aligned}
\frac{\partial \mathbf{u}_1}{\partial t} + y\mathbf{u}_1^{\perp} - \nabla\theta_1 &= 0, \\
\frac{\partial \theta_1}{\partial t} - \nabla\cdot\mathbf{u}_1 &= 0, \\
\frac{\partial q_{low}}{\partial t} + \sqrt{\frac{3}{2}}\left(\tilde{Q} + 2\sqrt{2}\bar{q}_2 - \frac{\bar{q}_1}{\sqrt{2}}\right)\nabla\cdot\mathbf{u}_1 &= 0, \\
\frac{\partial q_{mid}}{\partial t} + \sqrt{\frac{3}{2}}\left(\tilde{Q} + 2\sqrt{2}\bar{q}_2 + \frac{\bar{q}_1}{\sqrt{2}}\right)\nabla\cdot\mathbf{u}_1 &= 0.
\end{aligned} \tag{S12}$$

These equations are identical to the dynamical core in (1)–(4) of the main text if one makes the identification of

$$\tilde{Q}_{low} = \sqrt{\frac{3}{2}}\left(\tilde{Q} + 2\sqrt{2}\bar{q}_2 - \frac{\bar{q}_1}{\sqrt{2}}\right),$$
$$\tilde{Q}_{mid} = \sqrt{\frac{3}{2}}\left(\tilde{Q} + 2\sqrt{2}\bar{q}_2 + \frac{\bar{q}_1}{\sqrt{2}}\right), \tag{S13}$$

which completes the derivation.

Text S2. Moisture background profile

In this section, a background moisture profile, $q_{bg}(z)$, is associated with the two parameters $\tilde{Q}_{low}$ and $\tilde{Q}_{mid}$, in order to provide a physical interpretation of these parameters.

The background moisture profile, $q_{bg}(z)$, can be defined as

$$q_{bg}(z) = q_{00} - \tilde{Q}z + \bar{q}_1\sqrt{2}\sin z + \bar{q}_2 2\sqrt{2}\sin(2z), \tag{S14}$$

which includes both $q_{00} - \tilde{Q}z$ from the background part of q^{tot} in (S2) and $\bar{q}_1\sqrt{2}\sin z + \bar{q}_2 2\sqrt{2}\sin(2z)$ from the base state used in linearizing (S8) to obtain (S9).

First, one can derive a general relationship between (i) the derivative dq_{bg}/dz of the background moisture profile and (ii) the two parameters, $\tilde{Q}_{low}$ and $\tilde{Q}_{mid}$, in the following way. Start by considering vertical advection, as in (S1), applied to the background water vapor: $W dq_{bg}/dz$. If this is evaluated in the lower and middle troposphere at heights of $z = \pi/3$ and $z = 2\pi/3$, respectively, and if only the first baroclinic mode representation of $W = -(\nabla\cdot\mathbf{u}_1)\sqrt{2}\sin(z)$ is used, then the result is

$$\begin{aligned}
W\frac{dq_{bg}}{dz}\bigg|_{z=\pi/3} &= -(\nabla\cdot\mathbf{u}_1)\sqrt{2}\sin\left(\frac{\pi}{3}\right)\left[-\tilde{Q} + \bar{q}_1\sqrt{2}\cos\left(\frac{\pi}{3}\right) + \bar{q}_2 4\sqrt{2}\cos\left(2\frac{\pi}{3}\right)\right] \\
&= (\nabla\cdot\mathbf{u}_1)\sqrt{\frac{3}{2}}\left(\tilde{Q} - \frac{\bar{q}_1}{\sqrt{2}} + 2\sqrt{2}\bar{q}_2\right), \\
W\frac{dq_{bg}}{dz}\bigg|_{z=2\pi/3} &= -(\nabla\cdot\mathbf{u}_1)\sqrt{2}\sin\left(\frac{2\pi}{3}\right)\left[-\tilde{Q} + \bar{q}_1\sqrt{2}\cos\left(\frac{2\pi}{3}\right) + \bar{q}_2 4\sqrt{2}\cos\left(2\frac{2\pi}{3}\right)\right] \\
&= (\nabla\cdot\mathbf{u}_1)\sqrt{\frac{3}{2}}\left(\tilde{Q} + \frac{\bar{q}_1}{\sqrt{2}} + 2\sqrt{2}\bar{q}_2\right).
\end{aligned} \tag{S15}$$

These formulas can be identified with the terms $\tilde{Q}_{low}\nabla\cdot\mathbf{u}_1$ and $\tilde{Q}_{mid}\nabla\cdot\mathbf{u}_1$ from (S12) and (S13). Therefore, the physical interpretation of $\tilde{Q}_{low}$ and $\tilde{Q}_{mid}$ as the (scaled) derivative of the background moisture profile has been established:

$$\tilde{Q}_{low} = -\sqrt{\frac{3}{2}}\left.\frac{dq_{bg}}{dz}\right|_{z=\pi/3}, \tag{S16}$$

$$\tilde{Q}_{mid} = -\sqrt{\frac{3}{2}}\left.\frac{dq_{bg}}{dz}\right|_{z=2\pi/3}. \tag{S17}$$

Note that the $\sqrt{3/2}$ factor actually arises in this calculation from the vertical structure $\sqrt{2}\sin(z)$ of W, not from dq_{bg}/dz; it has nevertheless been absorbed into the definition of both $\tilde{Q}_{low}$ and $\tilde{Q}_{mid}$ in order to simplify notation.

Second, for the specific values of $\tilde{Q}_{low} = 0.9$ and $\tilde{Q}_{mid} = 0.45$ that are used in the present paper, what is the vertical structure of the associated background profile $q_{bg}(z)$? One assignment that is perhaps the simplest is the case of $\bar{q}_2 = 0$, in which case a one-to-one correspondence exists between $\tilde{Q}_{low}$ and $\tilde{Q}_{mid}$ on the one hand and $\tilde{Q}$ and $\bar{q}_1$ on the other:

$$\begin{aligned}\tilde{Q} &= \frac{\tilde{Q}_{low} + \tilde{Q}_{mid}}{\sqrt{6}} = 0.55,\\ -\bar{q}_1 &= \frac{\tilde{Q}_{low} - \tilde{Q}_{mid}}{\sqrt{3}} = 0.26,\end{aligned} \tag{S18}$$

which follows from (S13). A plot of $q_{bg}(z)$ with these values is shown in Fig. S4. This profile roughly resembles the water vapor profiles seen in nature [e.g., *Holloway and Neelin*, 2009], in that the most water vapor is in the lower troposphere, and both $q_{bg}(z)$ and dq_{bg}/dz decay with height. These features arise in the present context from the simple functional form of $q_{bg}(z) = \tilde{Q}(\pi - z) + \bar{q}_1\sqrt{2}\sin z$, a linear decay with z and a $\sin z$ part that contributes the convex shape that somewhat resembles exponential decay.

Note that the relationship between $\tilde{Q}_{low}$, $\tilde{Q}_{mid}$, and $q_{bg}(z)$ is not necessarily uniquely specified for this system with spectral truncation in the vertical. If, on the one hand, the background profile $q_{bg}(z)$ is given, in the form of (S14), then one can find the values of the parameters $\tilde{Q}_{low}$ and $\tilde{Q}_{mid}$ using (S13). If, on the other hand, only the two parameters $\tilde{Q}_{low}$ and $\tilde{Q}_{mid}$ are given, then many possible profiles $q_{bg}(z)$ are consistent with the given values of $\tilde{Q}_{low}$ and $\tilde{Q}_{mid}$; here we have assumed $\bar{q}_2 = 0$ as a simple way to select a reasonable case for illustration.

Text S3. Comparison with other models

To put the present model in perspective, we now compare it with some previous models. As a whole, the present model is new, to the best of our knowledge. Nevertheless, many individual components of the model are similar to some of the individual components of other models, as described briefly in the main text, and in more detail in what follows.

As a first example, the skeleton model of *Majda and Stechmann* [2009, 2011] produces an MJO with many realistic features [*Thual et al.*, 2014; *Ogrosky and Stechmann*, 2015a; *Stachnik et al.*, 2015; *Stechmann and Majda*, 2015]. The skeleton model is meant to represent intraseasonal- and planetary-scale dynamics; CCEWs appear on the smaller synoptic scales. The skeleton model and the present model utilize the same number of variables; in addition to their common use of first baroclinic mode velocity and potential temperature, the skeleton model includes a lower-tropospheric water vapor variable and a convective activity variable, whereas the present model includes lower- and mid-tropospheric water vapor variables. At a crude level of comparison, the convective activity variable a of the skeleton model is somewhat similar to the mid-tropospheric water vapor variable q_{mid} of the present model, although the $\tilde{Q}_{mid}$ term of the present model, which is important for obtaining a realistic MJO propagation speed in the present model, is

not included in the dynamics of a of the skeleton model. On the other hand, one could perhaps include a term like the Γqa term of a's dynamics into the q_{mid} dynamics here as a representation of vertical moisture fluxes.

As a second example, the multicloud model of *Khouider and Majda* [2006, 2007, 2008] has some parameter regimes that produce CCEWs with many realistic features. In other parameter regimes, the model can also produce waves that resemble the MJO [*Majda et al.*, 2007; *Khouider et al.*, 2011; *Ajayamohan et al.*, 2013], although the CCEW signatures do not simultaneously appear strongly with the MJO signature. At a crude level of comparison, the stratiform heating variable H_s of the multicloud model is somewhat similar to the mid-tropospheric water vapor variable q_{mid} of the present model, although the $\tilde{Q}_{mid}$ term of the present model, which is important for obtaining a realistic MJO propagation speed in the present model, is not included in the dynamics of H_s of the multicloud model. The multicloud model includes two vertical baroclinic modes of velocity and temperature, whereas the present model includes only one. Also, the multicloud model includes a troposphere-averaged water vapor variable and a boundary layer equivalent potential temperature variable, whereas the present model includes water vapor variables at two levels in the troposphere and no boundary layer variables.

As a third example, a convective adjustment model was analyzed by *Yu and Neelin* [1994], and planetary-scale moist mode was identified. The moist mode has a phase speed of roughly 14 m/s for wavenumber 1 and a dispersion relation that resembles a Kelvin wave [*Neelin and Yu*, 1994]. The model is similar to the present model in their common use of convective adjustment. However, many aspects are different. For example, the model used a single convective adjustment time scale of 2 hours for all vertical levels, whereas the present model uses different time scales of $O(2)$ hours and $O(1)$ day at different vertical levels. Stochastic forcing was investigated by *Yu and Neelin* [1994], and it was applied to the boundary-layer temperature equation or the boundary-layer kinematic equation, whereas the present paper included stochastic forcing in its free tropospheric water vapor equations.

As a fourth example, boundary-layer frictional convergence models for the MJO have also been investigated in various forms [e.g., *Wang and Rui*, 1990; *Salby et al.*, 1994]. Unstable modes are identified in these studies through the mechanisms of frictional wave–CISK (conditional instability of the second kind); in the present model, on the other hand, instabilities and boundary-layer frictional convergence are not included. Stochastic heating is also investigated by *Salby et al.* [1994], whereas stochastic moisture forcing is utilized in the present paper. Also, the frictional wave–CISK mechanism is active without dynamics of moisture, whereas moisture dynamics are a central part of the present paper.

As a fifth example, moisture mode models for the MJO emphasize and focus on the importance of water vapor [*Raymond and Fuchs*, 2009; *Sobel and Maloney*, 2013; *Adames and Kim*, 2016]. The models include a wide range of physical processes. The moisture mode models include, among several other physical processes described below, convective adjustment with time scales of 0.6 days [*Adames and Kim*, 2016] and 2.4 days [*Sobel and Maloney*, 2013]; these are somewhat similar to the mid-tropospheric adjustment time scale of 1.3 days used in the present study, the value of 4 days found via an analysis of the observed background spectrum of tropical convection [*Hottovy and Stechmann*, 2015], and the values of 0.5–2.0 days and 1.1 days that have been estimated in an analysis of global climate model and observational data, respectively [*Jiang et al.*, 2016]. Note that these estimates utilize column-averaged quantities, except for the the present model which distinguishes between lower- and mid-tropospheric water vapor. Also, *Sobel and Maloney* [2013] utilized eddy diffusion of moisture in the zonal direction, whereas the present model includes eddy diffusion of moisture in both the zonal and meridional directions. A wide range of additional physical processes are also included in moisture mode theory, such as cloud–radiation feedback, wind-induced surface heat exchange (WISHE) (or evaporation–wind feedback), boundary-layer frictional convergence, horizontal moisture advection by MJO-related high-frequency eddies, and horizontal moisture advection by large-scale winds. These additional processes contribute to the instability of moisture mode theory.

In the present model, on the other hand, these additional processes and instabilities are not explicitly included.

As a sixth example, moving-heat-source models have been investigated for the MJO [*Chao*, 1987; *Majda and Biello*, 2004; *Biello and Majda*, 2005] and for CCEWs [*Haertel and Kiladis*, 2004; *Majda and Biello*, 2004; *Biello and Majda*, 2005; *Stechmann et al.*, 2013]. In a moving-heat-source model, a diabatic heating function is prescribed, and the heating is moved at a prescribed speed. The movement of the heat source is meant to represent the wave's propagation, although this propagation or movement is prescribed in such a setup. Such a setup is an extension of the models of *Matsuno* [1966] and *Gill* [1980], who prescribed a steady, unmoving heat source in order to model the Walker and/or Hadley circulation. The value of moving-heat source models is in their descriptions of the MJO and CCEW structures, for the structures of the dry variables such as winds, temperature, and geopotential height. Results indicate that the structures of the MJO and some CCEWs can be modeled as the linear response to a moving heat source. However, such models do not predict the phase speeds or dispersion curves of the waves, since the propagation speed is prescribed. In contrast, in the model of the present paper, the MJO and CCEW heating is not prescribed. The heating in the present paper is modeled in terms of the water vapor, using a convective adjustment parameterization.

Text S4. Methods for determining model solutions

In this section, we describe how to determine semi-analytic solutions to the stochastic model in (1)–(4) of the main text.

In brief, in what follows, the equations are expanded in terms of the leading meridional basis functions of traditional equatorial wave theory, following *Matsuno* [1966], *Majda* [2003], and *Ogrosky and Stechmann* [2015b], and the water vapor equations are similarly expanded, following *Khouider and Majda* [2008], *Majda and Stechmann* [2009], and *Stechmann and Majda* [2015]. The result is a system of stochastic partial differential equations (SPDEs) as functions of x and t, which are linear with constant coefficients and can be solved using Fourier transforms [*Majda and Grote*, 2007, 2009; *Hottovy and Stechmann*, 2015].

Change to characteristic variables

It is convenient to change variables from the primitive (u, v, θ) variables to the characteristic variables (r, l, v):

$$r = \frac{1}{\sqrt{2}}(u - \theta), \quad l = \frac{1}{\sqrt{2}}(u + \theta). \tag{S19}$$

In terms of the variables (r, l, v), the model (1)–(2) from the main text takes the form

$$\begin{aligned} r_t + r_x + L_- v &= -\frac{1}{\tau} q - \frac{1}{\tau_r} r \\ l_t - l_x - L_+ v &= \frac{1}{\tau} q - \frac{1}{\tau_l} l \\ v_t + L_+ r - L_- l &= -\frac{1}{\tau_v} v, \end{aligned} \tag{S20}$$

where $L_\pm$ are the raising and lowering operators,

$$L_\pm = \frac{1}{\sqrt{2}}(\partial_y \pm y), \tag{S21}$$

and where we have defined

$$\frac{1}{\tau} q = \frac{1}{\sqrt{2}} \left(\frac{1}{\tau_{low}} q_{low} + \frac{1}{\tau_{mid}} q_{mid} \right) \tag{S22}$$

as an abbreviated notation. Also, here it is assumed that $\tau_u = \tau_\theta$ for simplicity, in which case $\tau_r = \tau_l = \tau_u$, and $\tau_v = \tau_u$.

Expansion in parabolic cylinder functions: Dry component equations

Next the variables are expanded in terms of meridional basis functions as

$$\begin{pmatrix} r(x,y,t) \\ l(x,y,t) \\ v(x,y,t) \\ q(x,y,t) \end{pmatrix} = \sum_{m=0}^{\infty} \begin{pmatrix} r_m(x,t) \\ l_m(x,t) \\ v_m(x,t) \\ q_m(x,t) \end{pmatrix} \phi_m(y), \tag{S23}$$

where the ϕ_m are the parablic cylinder functions,

$$\phi_m(y) = (m!\sqrt{\pi})^{-1/2} 2^{-m/2} H_m(y) e^{-y^2/2}, \tag{S24}$$

and where $H_m(y)$ are Hermite polynomials,

$$H_m(y) = (-1)^m e^{y^2} \frac{d^m}{dy^m} e^{-y^2}. \tag{S25}$$

To proceed further, equations are derived for the evolution of the coefficients $r_m(x,t)$, $l_m(x,t)$, etc. To derive equations for the coefficients $r_m(x,t)$, $l_m(x,t)$, etc., the equations for their parent variables $r(x,y,t)$, $l(x,y,t)$, etc. are projected onto each of the basis functions $\phi_m(y)$, using the fact that the parabolic cylinder functions $\phi_m(y)$ are an orthonormal basis. Another useful property is the effect of the operators $L_\pm$ on ϕ_m,

$$L_+\phi_m = \sqrt{m}\phi_{m-1}, \quad L_-\phi_m = -\sqrt{m+1}\phi_{m+1}, \tag{S26}$$

which indicates why $L_\pm$ are called the raising and lowering operators.

When the (r,l,v) system in (S20) is projected onto each of the basis functions $\phi_m(y)$, the result is three groups of equations. First is an equation for r_0,

$$\partial_t r_0 + \partial_x r_0 = -\frac{q_0}{\tau} - \frac{r_0}{\tau_r} \tag{S27}$$

which, in the absence of moisture q, would describe a Kelvin wave. Second is a coupled system for (r_1, v_0),

$$\begin{aligned} \partial_t r_1 + \partial_x r_1 - v_0 &= -\frac{q_1}{\tau} - \frac{r_1}{\tau_r} \\ \partial_t v_0 + r_1 &= -\frac{v_0}{\tau_v}, \end{aligned} \tag{S28}$$

which, in the absence of moisture q, would describe mixed Rossby–gravity waves. Third is an infinite family of systems involving the triplet (r_{m+1}, l_{m-1}, v_m) for $m \geq 1$,

$$\begin{aligned} \partial_t r_{m+1} + \partial_x r_{m+1} - \sqrt{m+1} v_m &= -\frac{q_{m+1}}{\tau} - \frac{r_{m+1}}{\tau_r} \\ \partial_t l_{m-1} - \partial_x l_{m-1} - \sqrt{m} v_m &= \frac{q_{m-1}}{\tau} - \frac{l_{m-1}}{\tau_l} \\ \partial_t v_m + \sqrt{m+1} r_{m+1} + \sqrt{m} l_{m-1} &= -\frac{v_m}{\tau_v}, \end{aligned} \tag{S29}$$

which, in the absence of moisture q, would describe an equatorial Rossby wave, a westward interio-gravity wave, and an eastward interio-gravity wave.

Expansion in parabolic cylinder functions: Moist component equations

To see the form of the q_{low} and q_{mid} equations when projected onto each of the basis functions $\phi_m(y)$, consider a generic equation

$$q_t + \tilde{Q}(u_x + v_y) = -\frac{1}{\tau} q + b(q_{xx} + q_{yy}) + F + D_* \dot{W}, \tag{S30}$$

which has the same mathematical form as the equations for q_{low} and q_{mid} in (3)–(4) of the main text. In this subsection, we use the notation q as a stand-in for either q_{low} or q_{mid}:

$$q = q_{low} \text{ or } q_{mid}. \tag{S31}$$

Note that this definition differs from the use of q in the derivation of the dry component equations for (r, l, v) above.

Some preliminary equivalences are useful for the derivation that follows. First, notice that the derivative ∂_y can be written in terms of the raising and lower operators as

$$L_+ + L_- = \sqrt{2}\partial_y, \tag{S32}$$

and u can be written in terms of characteristic variables r and l, so the divergence term can be written as

$$(u_x + v_y) = \frac{1}{\sqrt{2}}(r_x + l_x) + \frac{1}{\sqrt{2}}(L_+ + L_-)v. \tag{S33}$$

Second, note that the second derivative ∂_y^2 can be written as

$$\partial_y^2 = \frac{1}{2}(L_+ + L_-)^2 = \frac{1}{2}(L_+^2 + L_-^2 + L_+L_- + L_-L_+). \tag{S34}$$

Using these formulas, the moisture equation (S30) can be written in terms of parabolic cylinder functions.

The result, after projecting (S30) for the moisture dynamics onto parabolic cylinder function $\phi_m(y)$, is

$$\begin{aligned}
&\partial_t q_m + \frac{\tilde{Q}}{\sqrt{2}}\left[\partial_x r_m + \partial_x l_m + (\sqrt{m+1}v_{m+1} - \sqrt{m}v_{m-1})\right] \\
&\quad = -\frac{1}{\tau}q_m \\
&\qquad + b\partial_x^2 q_m + b\left(\frac{\sqrt{m(m-1)}}{2}q_{m-2} - \frac{2m+1}{2}q_m + \frac{\sqrt{(m+1)(m+2)}}{2}q_{m+2}\right) \\
&\qquad + F_m + D_*\dot{W}_m,
\end{aligned} \tag{S35}$$

where $\dot{W}_m(x,t)$ is spatiotemporal white noise, and $\dot{W}_m$ and $\dot{W}_{m'}$ are independent for $m \neq m'$. An equation of this form is used for each of $q_{low,m}(x,t)$ and $q_{mid,m}(x,t)$, with different coefficients $\tilde{Q}, \tau$, etc. for q_{low} versus q_{mid} according to their different equations in (3)–(4) of the main text.

Truncation of parabolic cylinder function expansion

For the dry component equations, the infinite family of systems from (S29) is truncated at a value of $m = M$, and the dynamics of the triplet (r_{M+1}, l_{M-1}, v_M) is fully retained. Such a choice ensures that the dynamics of the equatorial Rossby and inertio-gravity waves up to mode M are fully retained.

For the moist component equations, the variables $q_{low,m}$ and $q_{mid,m}$ are retained up to the value of $m = M - 1$.

For example, for a truncation with $M = 3$, the system is described by the following 18 variables:

$$\begin{aligned} &r_0, \\ &r_1, v_0, \\ &r_2, l_0, v_1, \\ &r_3, l_1, v_2, \\ &r_4, l_2, v_3, \\ &q_{low,0}, q_{low,1}, q_{low,2}, \\ &q_{mid,0}, q_{mid,1}, q_{mid,2}. \end{aligned} \tag{S36}$$

Results with the choice of $M = 3$ are used as the standard choice presented in the main text.

Vector formulation as system of SPDEs

The model takes the form of a system of stochastic partial differential equations (SPDEs). To write it in matrix-vector form, first define the column vector of all variables, which for $M = 3$ is

$$\mathbf{U}(x,t) = (r_0, r_1, v_0, r_2, l_0, v_1, r_3, l_1, v_2, r_4, l_2, v_3, q_{low,0}, q_{low,1}, q_{low,2}, q_{mid,0}, q_{mid,1}, q_{mid,2})^T, \tag{S37}$$

where ^{T} indicates the transpose operator. The dynamics of $\mathbf{U}$ can be assembled by considering the dynamics of each of its components, which were described above. In matrix–vector form, the dynamics is written as

$$\frac{\partial \mathbf{U}}{\partial t} + A\frac{\partial \mathbf{U}}{\partial x} = B\frac{\partial^2 \mathbf{U}}{\partial x^2} - C\mathbf{U} + \mathbf{F} + D\dot{\mathbf{W}}, \tag{S38}$$

where A, B, C, D are constant matrices, $\mathbf{F}$ is a vector, and $\dot{\mathbf{W}}$ is a vector whose components are independent spatiotemporal white noise terms.

Methods for determining eigenmodes

To determine the eigenvalues and eigenvectors of the unforced system, one assumes the ansatz of

$$\mathbf{U}(x,t) = \mathrm{Re}[\,\mathbf{U}_0 e^{i(kx-\omega t)}\,], \tag{S39}$$

where Re denotes the real part. Inserting this into (S38), in the absence of forcing, leads to

$$-i\omega\mathbf{U}_0 + ikA\mathbf{U}_0 = -k^2 B\mathbf{U}_0 - C\mathbf{U}_0, \tag{S40}$$

which defines an eigenvalue problem for eigenvalue $\omega(k)$ and eigenvector $\mathbf{U}_0(k)$.

Methods for computing solutions and statistics

Model solutions and their statistics can be computed semi-analytically. The model in (S38) is a system of SPDEs with constant coefficients and can be solved using Fourier transforms [*Majda and Grote*, 2007, 2009; *Hottovy and Stechmann*, 2015]. Two steps are used. First, a Fourier transform in space is applied to $\mathbf{U}(x,t)$, and each zonal wavenumber k can then be considered independently. Second, the solution vector $\hat{\mathbf{U}}(k,t)$ for wavenumber k is expanded in terms of the eigenvector basis, and each eigenvector amplitude can then be considered independently. The dynamics of each eigenmode is in the form of a complex Ornstein–Uhlenbeck (cOU) process, with a damping rate and oscillation frequency determined by the eigenmode's complex eigenvalue. The cOU process for each eigenmode can be solved analytically. The final solution $\mathbf{U}(x,t)$ or its statistics can then be assembled by combining the solutions for each

eigenmode and for each zonal wavenumber k. The solution is semi-analytic rather than analytic because only a finite number of zonal Fourier modes k is used and because the eigenvectors and eigenvalues are found using numerical linear algebra software.

The values of $F_{low}(x,y)$ and $F_{mid}(x,y)$ are chosen as idealized versions of moisture sources [e.g., *Ogrosky and Stechmann*, 2015a; *Stachnik et al.*, 2015], and they create a Walker circulation that aids the comparison between model output and observational data. To see the role of $F_{low}(x,y)$ and $F_{mid}(x,y)$, split the full solution $\mathbf{U}$ into two parts as

$$\mathbf{U}(x,t) = \bar{\mathbf{U}}(x) + \mathbf{U}'(x,t), \tag{S41}$$

where $\bar{\mathbf{U}}(x)$ is a time-independent mean component that represents the Walker circulation, and $\mathbf{U}'(x,t)$ is a time-dependent component that represents the wave variability including the MJO and CCEWs. Since the model is linear, one can split (S38) into two corresponding components:

$$\frac{\partial \mathbf{U}'}{\partial t} + A\frac{\partial \mathbf{U}'}{\partial x} = B\frac{\partial^2 \mathbf{U}'}{\partial x^2} - C\mathbf{U}' + D\dot{\mathbf{W}}, \tag{S42}$$

$$A\frac{\partial \bar{\mathbf{U}}}{\partial x} = B\frac{\partial^2 \bar{\mathbf{U}}}{\partial x^2} - C\bar{\mathbf{U}} + \mathbf{F}(x). \tag{S43}$$

In these two equations, the role of the forcing is split into its time-independent and time-dependent components, with the the steady deterministic $\mathbf{F}(x)$ generating the steady deterministic Walker circulation, and with the random forcing $D\dot{\mathbf{W}}$ generating the wave variability. In the main text, Fig. 1 includes the mean Walker circulation that is created by the steady moisture sources $F_{low}(x,y)$ and $F_{mid}(x,y)$, in order to compare with the analogous plot from observational data [*Zhang*, 2005] which includes the Walker circulation. On the other hand, note that Figs. 2–4 are not influenced by $F_{low}(x,y)$ and $F_{mid}(x,y)$; in creating the steady Walker circulation, $F_{low}(x,y)$ and $F_{mid}(x,y)$ affect the means but not the variances of the model variables. To illustrate the model's wave variability alone, Fig. S5 is a reproduction of the Fig. 1 of the main text, except with $F_{low}(x,y)$ and $F_{mid}(x,y)$ set to zero to remove the mean Walker circulation; the wave variability in Fig. 1 and Fig. S5 is identical, since the steady Walker circulation is independent from the wave variability, due to the model's linearity. For simplicity, we take identical values $F_{low}(x,y) = F_{mid}(x,y) = F(x,y)$, and we take $F(x,y) = F_0(x)\phi_0(y)$, where $\phi_0(y)$ is the $m = 0$ parabolic cylinder function. The function $F_0(x)$ is chosen as

$$F_0(x) = F_* \left[\exp\left(\frac{-(x-n_1)^4}{2\sigma_1} \right) + \frac{3}{4}\exp\left(\frac{-(x-n_2)^4}{2\sigma_2} \right) - \frac{1}{2} \right], \tag{S44}$$

which creates two plateaus of moisture sources, in alignment with the two moist, ascending branches of the "global" Walker circulation [*Stechmann and Ogrosky*, 2014; *Ogrosky and Stechmann*, 2015a]. The parameters are $n_1 = (1/3) \times 40{,}000$ km, $n_2 = (5/6) \times 40{,}000$ km, $\sigma_1 = 0.003$ km^4, $\sigma_2 = 0.0001$ km^4, and $F = 1.1055 \times 10^{-5}$ (kg/kg) h^{-1}.

As mentioned above, all eigenmodes are damped and stable in the standard parameter regime. If the moisture diffusion were ignored by setting $b_{low} = b_{mid} = 0$, with all other parameters taking their standard values here, then some eigenmodes would become unstable, and their growth rates would be largest for the smallest spatial scales, but their growth rates would be bounded (i.e., there is no "ultraviolet catastrophe"). Since the standard parameter regime has eigenmodes that are all damped and stable, the stochastic version of the model has a well-defined stationary state (i.e., climatological mean state), whose rainfall variability is characterized by the power spectrum in Fig. 3 of the main text. The values of b_{low} and b_{mid} impact the shape of the power spectrum in a way that is similar to the results of *Hottovy and Stechmann* [2015]; namely, their main influence is in shaping the power spectrum's decay as the wavenumber k increases, which decays roughly as $\sim k^{-2}$. The damping parameters τ_u, τ_v, and τ_θ of the dry dynamical variables have a less significant impact on the shape of the precipitation power spectrum.

In the lag-lead regression plots in Fig. 2, in order to give dimensional units to all quantities, the base time series of precipitation has been scaled and nondimensionalized so that the

result of the self-regression with precipitation has a maximum amplitude of 5 mm/day. Also, for the contoured variables, the minimum and maximum values are, respectively, a) -14.37 and 10.86 m, b) -2.43 and 2.21 m, c) -0.15 and 0.21 K, and d) -0.13 and 0.14 K.

Also, in the eigenvector plots in Fig. 4, in order to give dimensional units to all quantities, the arbitrary overall amplitude of the eigenvector has been chosen so that the precipitation has a maximum amplitude of 5 mm/day. Also, for the contoured variables, the maximum values are a) 16.61 m, b) 5.64 m, c) 0.17 K, and d) 0.3 K; and the maximum wind speeds in the x and/or y and/or z directions are a) x-7.61 m/s, y-0.69 m/s, b) x-0.66 m/s, y-0.07 m/s, c) x-7.74 m/s, z-1.85 cm/s, d)x-0.88 m/s, z-0.35 cm/s.

In the plot of the alternative CCKW eigenvector in Fig. S1a, the maximum geopotential height value is 5.0 m, and the maximum zonal and meridional wind speeds are 1.73 and 0.77 m/s.

Finally, note that the time axis in Fig. 1 is labelled using months (January, February, March, etc.), but no seasonal cycle is included in the model.

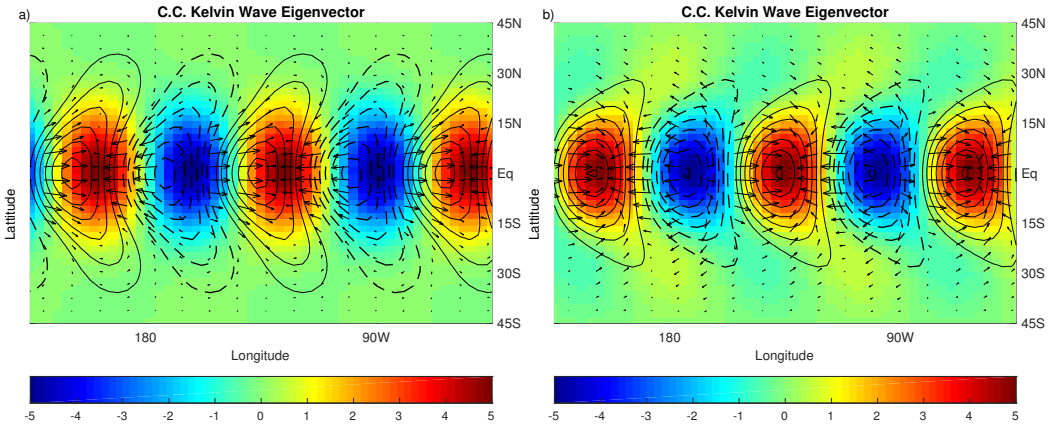

Figure S1. Two eigenmodes that resemble the convectively coupled Kelvin wave structure seen in the statistical composite in Fig. 2b of the main text. Zonal wavenumber $k = 5$. Geopotential height contour intervals are 0.56 m. The eigenmode in panel b is also shown in the main text in Fig. 4b. Phase speeds are (a) 13.4 m/s and (b) 18.5 m/s.

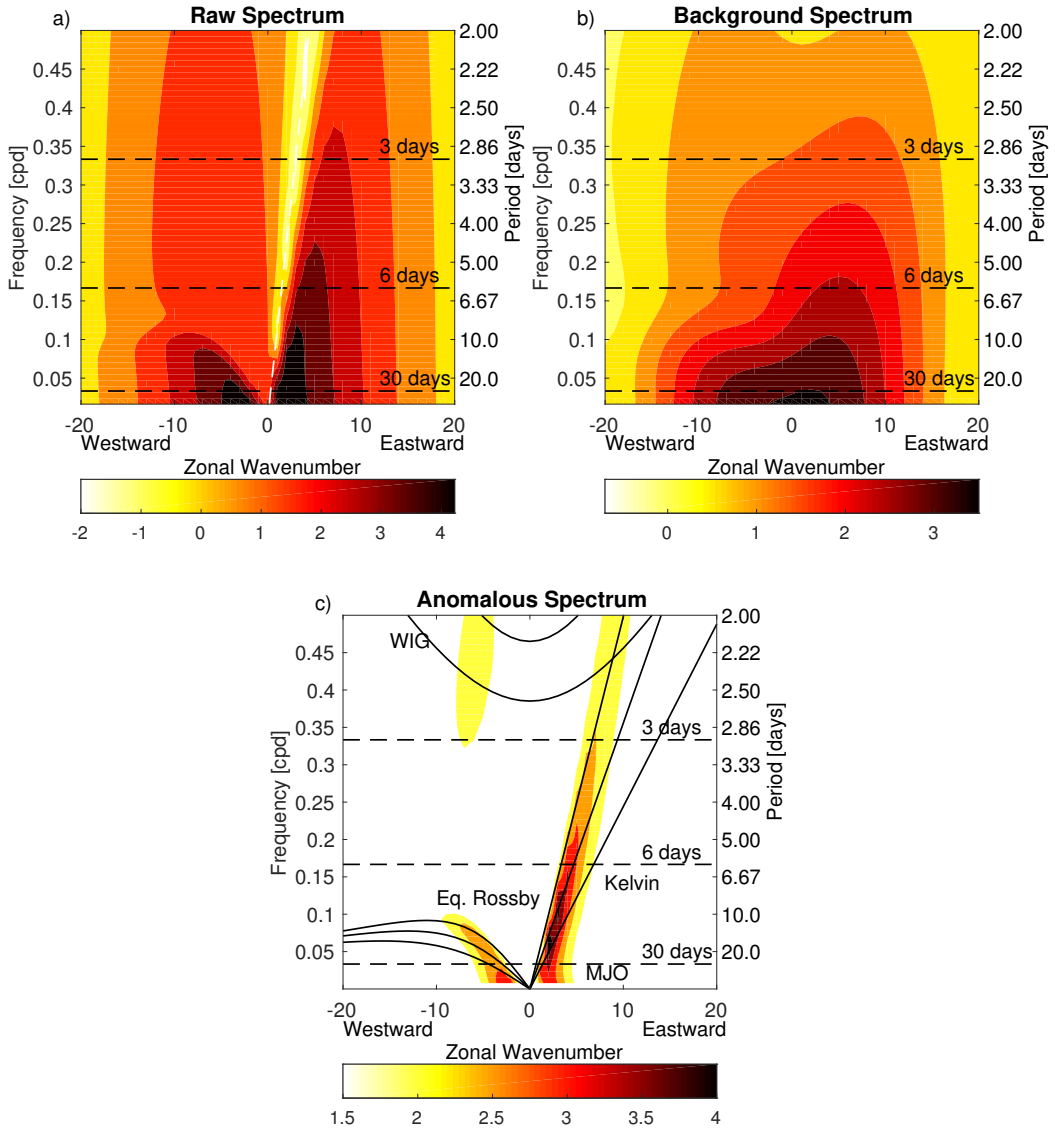

Figure S2. Same as Fig. 3 of the main text, except for hybrid MJO–Kelvin wave case, as described in section 5 of the main text. Same parameter values as the standard case, except a lower value of $\tilde{Q}_{mid} = 0.1$ is used, in comparison to the standard value of $\tilde{Q}_{mid} = 0.45$.

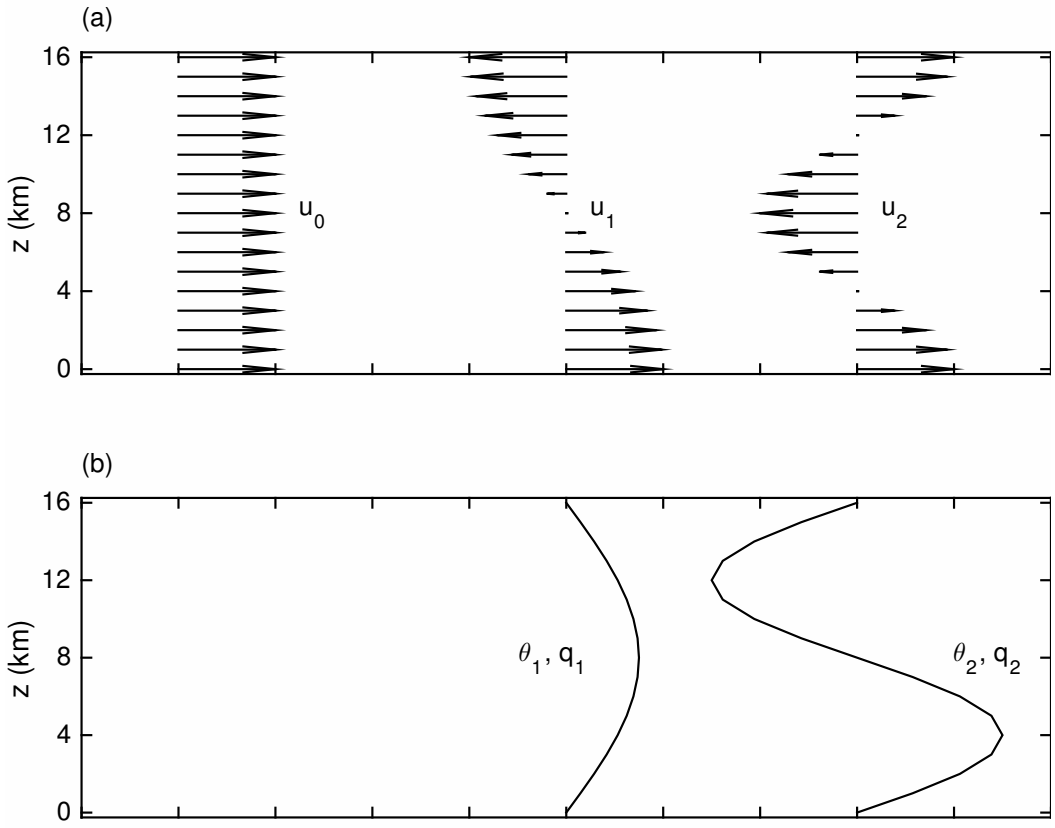

Figure S3. Vertical profiles for the first few modes of (a) velocity and (b) potential temperature and water vapor, as described in (S3) and (S5). Adapted from *Stechmann et al.* [2008].

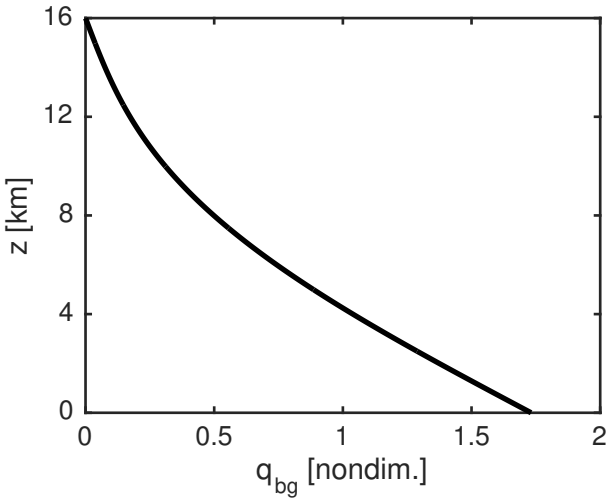

Figure S4. Background profile $q_{bg}(z)$ of water vapor.

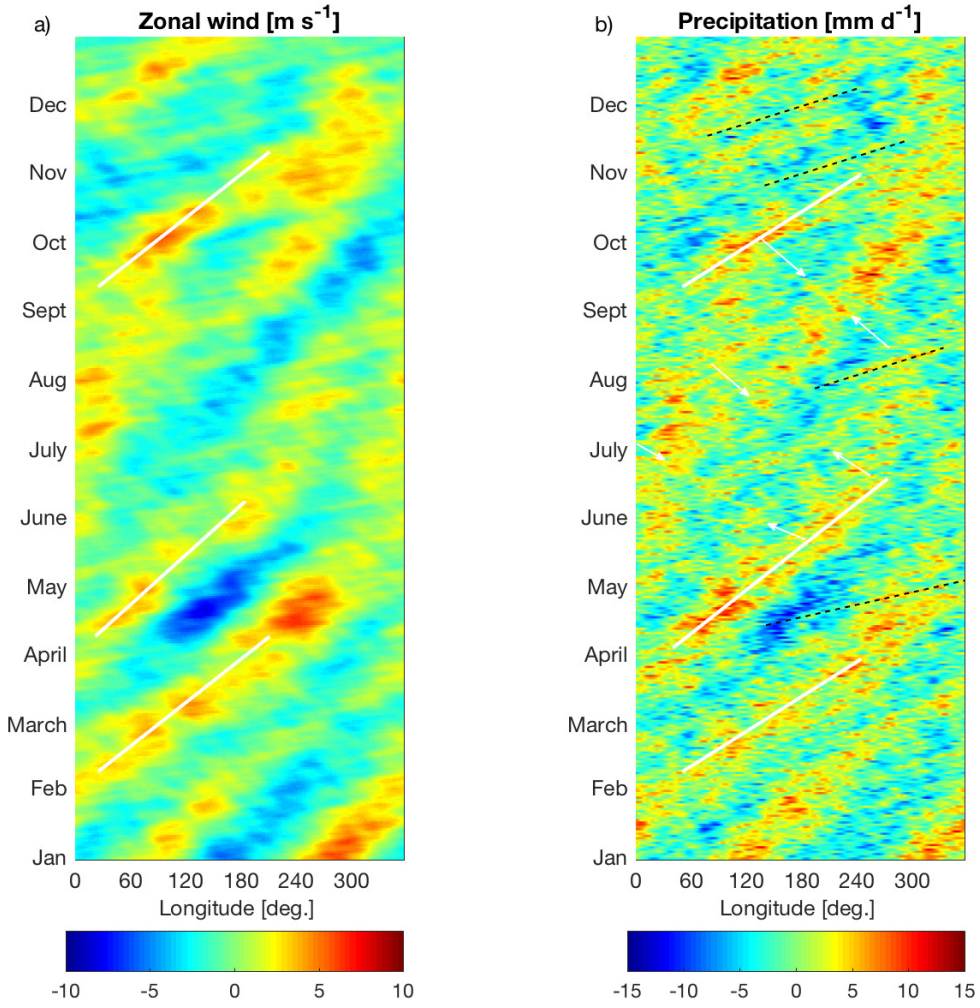

Figure S5. Same as Fig. 1 of the main text, except with the steady Walker circulation removed by setting $F_{low}(x, y) = F_{mid}(x, y) = 0$.

References

Adames, Á. F., and D. Kim (2016), The MJO as a dispersive, convectively coupled moisture wave: Theory and observations, *J. Atmos. Sci.*, *73*(3), 913–941.

Ajayamohan, R. S., B. Khouider, and A. J. Majda (2013), Realistic initiation and dynamics of the Madden–Julian Oscillation in a coarse resolution aquaplanet GCM, *Geophys. Res. Lett.*, *40*(23), 6252–6257.

Biello, J. A., and A. J. Majda (2005), A new multiscale model for the Madden–Julian oscillation., *J. Atmos. Sci.*, *62*, 1694–1721.

Chao, W. C. (1987), On the origin of the tropical intraseasonal oscillation., *J. Atmos. Sci.*, *44*, 1940–1949.

Gill, A. E. (1980), Some simple solutions for heat-induced tropical circulation, *Q. J. Royal Meteor. Soc.*, *106*(449), 447–462.

Haertel, P. T., and G. N. Kiladis (2004), Dynamics of 2-day equatorial waves., *J. Atmos. Sci.*, *61*, 2707–2721.

Holloway, C. E., and J. D. Neelin (2009), Moisture vertical structure, column water vapor, and tropical deep convection, *J. Atmos. Sci.*, *66*(6), 1665–1683.

Hottovy, S. A., and S. N. Stechmann (2015), A spatiotemporal stochastic model for tropical precipitation and water vapor dynamics, *J. Atmos. Sci.*, *72*, 4721–4738, doi: 10.1175/JAS-D-15-0119.1.

Jiang, X., M. Zhao, E. D. Maloney, and D. E. Waliser (2016), Convective moisture adjustment time scale as a key factor in regulating model amplitude of the Madden-Julian oscillation, *Geophys. Res. Lett.*, *43*(19).

Khouider, B., and A. J. Majda (2006), A simple multicloud parameterization for convectively coupled tropical waves. Part I: Linear analysis, *J. Atmos. Sci.*, *63*, 1308–1323.

Khouider, B., and A. J. Majda (2007), A simple multicloud parameterization for convectively coupled tropical waves. Part II: Nonlinear simulations, *J. Atmos. Sci.*, *64*, 381–400.

Khouider, B., and A. J. Majda (2008), Equatorial convectively coupled waves in a simple multicloud model, *J. Atmos. Sci.*, *65*, 3376–3397.

Khouider, B., A. St-Cyr, A. J. Majda, and J. Tribbia (2011), The MJO and convectively coupled waves in a coarse-resolution GCM with a simple multicloud parameterization, *J. Atmos. Sci.*, *68*, 240–264.

Majda, A. J. (2003), *Introduction to PDEs and Waves for the Atmosphere and Ocean*, *Courant Lecture Notes in Mathematics*, vol. 9, x+234 pp., American Mathematical Society, Providence.

Majda, A. J., and J. A. Biello (2004), A multiscale model for the intraseasonal oscillation, *Proc. Natl. Acad. Sci. USA*, *101*(14), 4736–4741.

Majda, A. J., and M. J. Grote (2007), Explicit off-line criteria for stable accurate time filtering of strongly unstable spatially extended systems, *Proc. Natl. Acad. Sci. USA*, *104*, 1124–1129.

Majda, A. J., and M. J. Grote (2009), Mathematical test models for superparametrization in anisotropic turbulence, *Proc. Natl. Acad. Sci. USA*, *106*(14), 5470–5474.

Majda, A. J., and S. N. Stechmann (2009), The skeleton of tropical intraseasonal oscillations, *Proc. Natl. Acad. Sci. USA*, *106*(21), 8417–8422.

Majda, A. J., and S. N. Stechmann (2011), Nonlinear dynamics and regional variations in the MJO skeleton, *J. Atmos. Sci.*, *68*, 3053–3071.

Majda, A. J., S. N. Stechmann, and B. Khouider (2007), Madden–Julian Oscillation analog and intraseasonal variability in a multicloud model above the equator, *Proc. Natl. Acad. Sci. USA*, *104*(24), 9919–9924.

Matsuno, T. (1966), Quasi-geostrophic motions in the equatorial area, *J. Meteor. Soc. Japan*, *44*(1), 25–43.

Neelin, J. D., and J.-Y. Yu (1994), Modes of tropical variability under convective adjustment and the Madden–Julian oscillation. Part 1: Analytical theory, *J. Atmos. Sci.*, *51*,

1876–1894.

Ogrosky, H. R., and S. N. Stechmann (2015a), The MJO skeleton model with observation-based background state and forcing, *Q. J. Roy. Meteor. Soc.*, *141*(692), 2654–2669, doi:10.1002/qj.2552.

Ogrosky, H. R., and S. N. Stechmann (2015b), Assessing the equatorial long-wave approximation: asymptotics and observational data analysis, *J. Atmos. Sci.*, *72*, 4821–4843, doi:10.1175/JAS-D-15-0065.1.

Raymond, D. J., and Ž. Fuchs (2009), Moisture modes and the Madden–Julian oscillation, *J. Climate*, *22*(11), 3031–3046.

Salby, M. L., R. R. Garcia, and H. H. Hendon (1994), Planetary-scale circulations in the presence of climatological and wave-induced heating., *J. Atmos. Sci.*, *51*, 2344–2367.

Sobel, A., and E. Maloney (2013), Moisture modes and the eastward propagation of the MJO, *J. Atmos. Sci.*, *70*(1), 187–192.

Stachnik, J. P., D. E. Waliser, A. J. Majda, S. N. Stechmann, and S. Thual (2015), Evaluating MJO event initiation and decay in the skeleton model using an RMM-like index, *J. Geophys. Res. Atmos.*, *120*(22), doi:10.1002/2015JD023916.

Stechmann, S. N., and A. J. Majda (2015), Identifying the skeleton of the Madden–Julian oscillation in observational data, *Mon. Wea. Rev.*, *143*, 395–416, doi:10.1175/MWR-D-14-00169.1.

Stechmann, S. N., and H. R. Ogrosky (2014), The Walker circulation, diabatic heating, and outgoing longwave radiation, *Geophys. Res. Lett.*, *41*, 9097–9105, doi:10.1002/2014GL062257.

Stechmann, S. N., A. J. Majda, and B. Khouider (2008), Nonlinear dynamics of hydrostatic internal gravity waves, *Theor. Comp. Fluid Dyn.*, *22*, 407–432.

Stechmann, S. N., A. J. Majda, and D. Skjorshammer (2013), Convectively coupled wave–environment interactions, *Theor. Comp. Fluid Dyn.*, *27*, 513–532.

Thual, S., A. J. Majda, and S. N. Stechmann (2014), A stochastic skeleton model for the MJO, *J. Atmos. Sci.*, *71*, 697–715.

Wang, B., and H. Rui (1990), Dynamics of the coupled moist Kelvin–Rossby wave on an equatorial beta-plane., *J. Atmos. Sci.*, *47*, 397–413.

Yu, J.-Y., and J. D. Neelin (1994), Modes of tropical variability under convective adjustment and the Madden–Julian oscillation. Part II: Numerical results, *J. Atmos. Sci.*, *51*(13), 1895–1914.

Zhang, C. (2005), Madden–Julian Oscillation, *Rev. Geophys.*, *43*, RG2003, doi:10.1029/2004RG000158.